

Full length article

# Viscoelastic properties of the equine hoof wall

Christian Bonney<sup>a</sup>, Siyuan Pang<sup>a</sup>, Marc A. Meyers<sup>b,c,d</sup>, Iwona Jasiuk<sup>a,\*</sup><sup>a</sup> Department of Mechanical Science and Engineering, University of Illinois Urbana-Champaign, USA<sup>b</sup> Materials Science and Engineering Program, University of California San Diego, USA<sup>c</sup> Department of Mechanical and Aerospace Engineering, University of California San Diego, USA<sup>d</sup> Department of Nanoengineering, University of California, San Diego, USA

## ARTICLE INFO

### Article history:

Received 27 January 2024

Revised 12 June 2024

Accepted 13 June 2024

Available online 20 June 2024

### Keywords:

Hoof wall

Viscoelasticity

Dynamic mechanical analysis

Biological material

Nanoindentation

Impact resistance

## ABSTRACT

The equine hoof wall has outstanding impact resistance, which enables high-velocity gallop over hard terrain with minimum damage. To better understand its viscoelastic behavior, complex moduli were determined using two complementary techniques: conventional (~5 mm length scale) and nano (~1 μm length scale) dynamic mechanical analysis (DMA). The evolution of their magnitudes was measured for two hydration conditions: fully hydrated and ambient. The storage modulus of the ambient hoof wall was approximately 400 MPa in macro-scale experiments, decreasing to ~250 MPa with hydration. In contrast, the loss tangent decreased for both hydrated (~0.1–0.07) and ambient (~0.04–0.01) conditions, over the frequency range of 1–10 Hz. Nano-DMA indentation tests conducted up to 200 Hz showed little frequency dependence beyond 10 Hz. The loss tangent of tubular regions showed more hydration sensitivity than in intertubular regions, but no significant difference in storage modulus was observed. Loss tangent and effective stiffness were higher in indentations for both hydration levels. This behavior is attributed to the hoof wall's hierarchical structure, which has porosity, functionally graded aspects, and material interfaces that are not captured at the scale of indentation. The hoof wall's viscoelasticity characterized in this work has implications for the design of bioinspired impact-resistant materials and structures.

### Statement of significance

The outer wall of horse hooves evolved to withstand heavy impacts during gallop. While previous studies have measured the properties of the hoof wall in slowly changing conditions, we wanted to quantify its behavior using experiments that replicate the quickly changing forces of impact. Since the hoof wall's structure is complex and contributes to its overall performance, smaller scale experiments were also performed. The behavior of the hoof wall was within the range of other biological materials and polymers. When hydrated, it becomes softer and can dissipate more energy. This work improves our understanding of the hoof's function and allows for more accurate simulations that can account for different impact speeds.

© 2024 The Author(s). Published by Elsevier Ltd on behalf of Acta Materialia Inc.

This is an open access article under the CC BY license (<http://creativecommons.org/licenses/by/4.0/>)

## 1. Introduction

The equine hoof wall is a keratinous structure that evolved under impact loading and thus has attracted interest in the field of bioinspiration. Researchers have achieved improved fracture toughness and crashworthiness from structures inspired by the hoof wall [1–4]. However, the role of viscoelasticity in its mechanical function has been less extensively studied. Like other non-mineralized

biological materials, the hoof wall exhibits notable viscoelastic behavior such as strain-rate sensitivity, stress relaxation, and creep [4–6]. These experiments offer insights into the material behavior under quasistatic or slowly changing conditions, but further characterization is needed for the dynamic response at shorter time scales that are relevant to impact loading. In this paper, the linear viscoelastic properties of the hoof wall are characterized by dynamic mechanical analysis (DMA) accounting for hydration, loading direction, and structural scale.

DMA is a common technique for characterizing the viscoelastic properties of polymers, gels, elastomers, and biological tissues [7–11]. This method works by applying an oscillatory stress or strain and measuring the phase lag ( $\delta$ ) in the material's response. The

\* Corresponding author at: Department of Mechanical Science and Engineering, University of Illinois Urbana-Champaign, 1206 West Green Street, Urbana, IL 61801, USA.

E-mail address: [ijasiuk@illinois.edu](mailto:ijasiuk@illinois.edu) (I. Jasiuk).

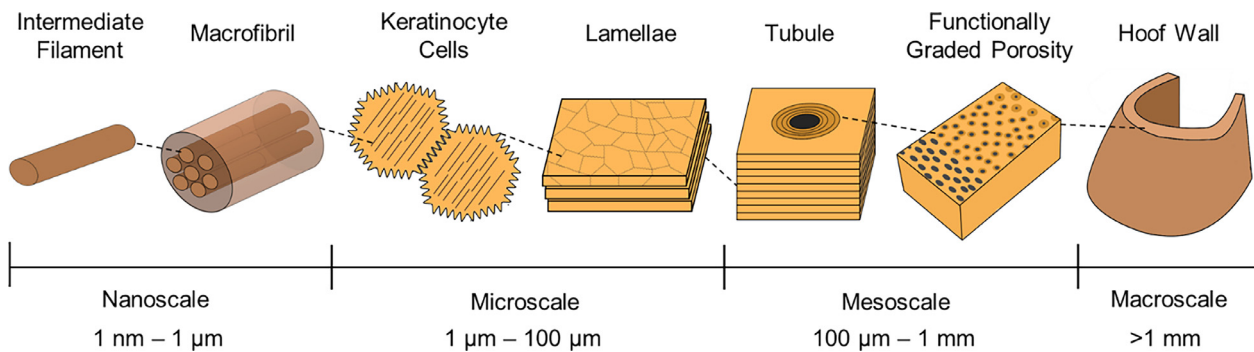


Fig. 1. Hierarchical structure of equine hoof wall.

stress-strain relationship under this loading can be described by the complex modulus ( $E^*$ ), defined by:

$$E^* = E' + iE'' \quad (1)$$

where the storage modulus ( $E'$ ) represents the material's ability to store energy elastically and the loss modulus ( $E''$ ) represents the material's energy dissipation through viscous flow. They are defined as:

$$E' = \frac{\sigma_0}{\varepsilon_0} \cos(\delta) \quad (2)$$

$$E'' = \frac{\sigma_0}{\varepsilon_0} \sin(\delta) \quad (3)$$

where  $\sigma_0$  and  $\varepsilon_0$  are the stress and strain amplitudes, respectively. The magnitude of the complex modulus,  $|E^*|$ , represents the material's stiffness or Young's modulus and the loss tangent ( $\tan(\delta)$ ) is the ratio of the loss modulus to the storage modulus, indicating the relative contributions of viscous and elastic behaviors [12,40]. In nano-DMA, an oscillatory load is applied by an indenter, and the resulting force-displacement response is measured. The complex modulus is a function of the contact stiffness, phase lag, and indenter geometry [13].

Using DMA, the hoof wall's dynamic properties can be quantified for loading rates comparable to a typical impact with the ground. Based on acceleration measurements from the hooves of trotting horses, the impact velocity is 1–6 m/s [14,15] and the duration of contact with the ground is 200–300 ms [15]. Taking the inverse of contact duration, the frequency of the stress wave imparted during impact can be estimated as 3.3–5 Hz. For a full gallop, this increases to 6.7–13.3 Hz [16] making 10 Hz a reasonable upper bound for dynamic frequency measurements. The frequency sweep data from macroscale DMA (1–10 Hz) and nano-DMA (1–200 Hz) should therefore capture most of the relevant viscoelastic behavior for *in vivo* deformation. Impact also results in vibrations of much higher frequencies (200–600 Hz) [17] but the response in this range must be inferred from lower frequency tests due to equipment limitations. This dynamic response will improve finite element studies of the hoof wall, which previously used linear elastic and hyperelastic models based on quasistatic experiments [18–21].

The damping characteristics of the hoof wall need to be studied in the context of its hierarchical structure (Fig. 1). The hoof wall is made of  $\alpha$ -keratin [22], which is composed of an amorphous protein matrix and crystalline intermediate filaments (IFs) about 7 nm in diameter [23]. Cells, containing aligned bundles of IFs or macrofibrils, combine to form lamellae with a thickness of 5–15  $\mu\text{m}$  [24]. The lamellar structure is populated with semi-hollow elliptical tubules, parallel to the outer surface of the hoof wall or longitudinal direction. The tubular region consists of the tubule wall, formed by 7–10 concentric cortical lamellae, and the central

medullary cavity, which is partially filled by tissue and bridging structures [4,24,25]. The intertubular region refers to the remaining parallel lamellae between tubules [24,26]. Tubules vary in size and density depending on their location along the hoof wall thickness or radial direction, resulting in a functionally graded structure [27,28]. Those near the exterior of the hoof wall, or stratum externum, have a density of 15  $\text{mm}^{-2}$  and a major diameter of 245  $\mu\text{m}$ . The density and diameter decrease to 5  $\text{mm}^{-2}$  and 200  $\mu\text{m}$  near the interior, or stratum internum. Tubule medullary cavities vary in diameter from 36 to 70  $\mu\text{m}$  resulting in a porosity of about 3–4 %, but the overall porosity of the material increases to ~8 % when nano-sized pores are considered [24,25,28]. Because of its heterogeneity, the hoof wall is divided into medial, toe, and lateral sections along its curvature or circumferential direction. Most studies on the mechanical properties of the hoof wall, including this work, use samples from the toe region due to its superior stiffness, larger thickness for collecting samples, and more direct comparison to prior research.

In a living horse, the hoof wall tissue at the stratum internum is directly exposed to body fluids while the material near the stratum externum is exposed to the ambient air and is relatively dry by comparison. These conditions create a hydration gradient in the same direction as the morphological gradient of the tubules. Researchers typically control the water content of hoof wall samples since mechanical properties are known to vary with hydration. When fully hydrated, the hoof wall is up to 35 times more compliant than in a dry state [26]. Likewise, creep and relaxation tests revealed a general increase in viscous effects with additional hydration [4]. Exact *in vivo* hydration levels are unknown but based on measurements from harvested samples, the outer ambient material is about 17–24 % water by weight. When fully hydrated, like the material at the stratum internum, the water content increases to 30–40 % [27].

In this work, nano-DMA and DMA compression tests at different loading directions and hydration levels give information on the relationship between the hierarchical structure and mechanical properties that can inform the design of impact resistant materials inspired by the hoof wall.

## 2. Methods

Hooves from five deceased Quarter Horses were provided by the University of Illinois Urbana-Champaign and University of California, Davis veterinary medicine departments. For each animal, all four hooves were removed above the ankle and refrigerated for less than 48 h before being frozen at  $-20^\circ\text{C}$ . The hooves were cut below the coronary band and separated from the frog and sole with a bandsaw before removing the hoof wall with a knife. All samples came from the toe region of the stratum medium as shown in Fig. 2. The longitudinal (L), radial (R), and circumferential

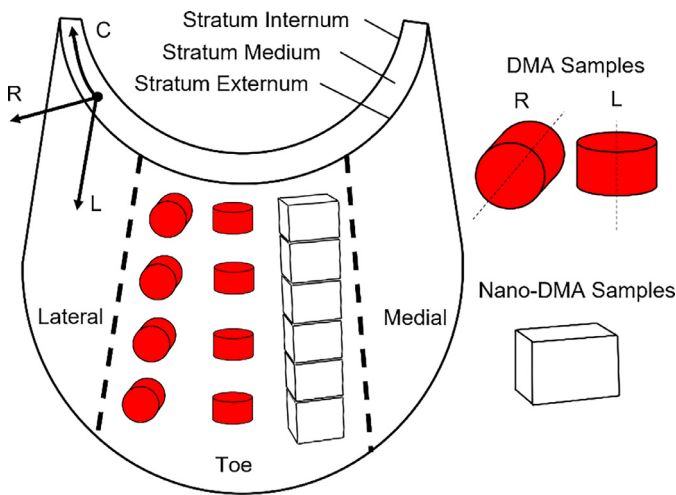


**Fig. 2.** Front view of hoof wall showing sample orientations. The longitudinal direction is parallel with the hoof's outer lateral surface. The radial direction is normal to the hoof's surface and points in the thickness direction. The circumferential direction points along the curvature of the hoof wall.

(C) directions are used to describe sample orientation, as well as the loading direction of the experiment.

Fully hydrated samples were tested underwater and submerged at least four days prior to the test. Ambient samples were tested in the ambient conditions of the laboratory (27–40 % relative humidity) and never hydrated. After testing, samples were dried in an oven at 101 °C until their weight reached a constant value ensuring that most of the water in the samples had evaporated. The water content by weight was calculated by comparing the weight of dry samples to their weight during testing. Ambient samples had a water content of  $18 \pm 3$  % while fully hydrated samples had a water content of  $35 \pm 4$  %.

### 2.1. DMA

Cylindrical DMA samples, approximately 5 mm in diameter and 7 mm height, were extracted from the hoof wall of two horses with a core drill bit. The axes of the cylindrical samples were parallel to the intended loading direction (L or R). The ends were polished to ensure suitably flat and parallel faces for DMA compression. After discarding samples with defects or incorrect dimensions, the remaining were randomly assigned to either fully hydrated or ambient hydration levels making four experimental groups, each with at least 5 samples.

Sinusoidal compressive loading was applied using a Bose Electroforce 3200 dynamic mechanical analyzer (TA Instruments, New Castle, DE, USA). All tests were performed under load control to avoid losing contact with the sample. First, an amplitude sweep at a constant frequency of 1 Hz was performed to ensure samples remained in the linear viscoelastic region. Based on amplitude sweeps of hydrated and dry samples, a dynamic amplitude of 30 N was chosen for all experiments. At this amplitude, the strain did not exceed 0.01 for any sample. Samples were then tested under a frequency sweep from 1 to 10 Hz. This range was chosen to avoid resonances in the machine-sample system at higher frequencies, which is a common source of error in DMA [29]. Preliminary experiments on a wider frequency range (5–200 Hz) encountered error due to resonance above 25 Hz.

### 2.2. Nano-DMA

Longitudinal strips were extracted from the hoof walls of three horses with a band saw. About 5 mm tall samples were cut us-

ing a diamond sectioning saw (Isomet 1000, Buehler, Lake Bluff, IL, USA) so that the indenting direction was along the longitudinal direction. Sample surfaces were polished using a speed grinder with sandpapers ranging in roughness from 30  $\mu\text{m}$  to 1  $\mu\text{m}$ . A finer surface polish was performed using a Syntron vibratory polisher with 50 nm alumina powders in fluid overnight. After polishing, samples were randomly assigned to either ambient or fully hydrated conditions.

The Hysitron TI-950 Triboindenter (Bruker, Billerica, MA, USA) was used to perform nano-DMA in frequency sweeping mode with a Berkovich tip. The nano-DMA transducer was calibrated by indenting the tip in the air. "H" pattern indentation was performed on an aluminum foil to calibrate optics and probe offset. The tip area function was calibrated with a standard quartz sample with a known elastic modulus. After completing all the calibration, samples were mounted onto a steel holder using super glue.

To perform indentation in fluid, samples were first glued to the middle of a Petri dish using a cyanoacrylate-based glue. Deionized (DI) water was then gently poured into the Petri dish using a pipette until the horizontal level of DI water was  $\sim 2$  mm above the sample surface. Calibration and experiments at the fully hydrated level were performed underwater. Due to the light scatter, a 15 mN setpoint was applied to ensure the tip could approach the sample surface. A 2 min dwell time was performed to reduce tip drifting due to vertical movement in fluids. A 10 mN preload followed by a 500 mN load with a rate of 100 mN/s was applied for both indentation levels to ensure indenting was performed at a depth of at least 200 nm inside the sample surface, allowing more direct comparison to previous indentation experiments [5]. Then, after a 2 s quasi-static dwell time, the probe started the oscillations, sweeping the frequency from 1 to 200 Hz at 20 intervals. For each hydration level, six samples were indented in three tubular regions and three intertubular regions. Indentation locations were selected arbitrarily but remained in the center of the hoof wall thickness rather than near the stratum internum or stratum externum.

### 2.3. Statistical methods

A four-way analysis of variance (ANOVA) was employed to determine which variables had a significant effect on the measurements of complex moduli. Barlett's test was used to verify homogeneity of variance within each group, an assumption of ANOVA. Results of the analysis are shown in Table 1 to quantify the significance and effect size of each factor.

## 3. Results and discussion

### 3.1. DMA

Frequency sweep results for macroscale DMA are shown in Fig. 3a and b. With increasing frequency, the storage modulus increased while the loss tangent decreased. The hoof wall therefore behaves more elastically at higher loading frequencies, mirroring the behavior observed in prior tension DMA experiments on hair [30].

Results from nano-DMA illustrate how the effective stiffness of the hoof wall tends to increase at smaller scales as pointed out by [31]. For the frequencies shared between the two methods, both loss tangent and storage modulus measured from indentation were higher than those given by compression. The contact area for the indenter was around 1  $\mu\text{m}^2$  so the additional compliance introduced by cell boundaries, lamellar interfaces, and tubule porosity was not captured leading to an order of magnitude higher measured storage modulus. These results also indicate that the interfaces behave more elastically than the rest of the material, resulting in reduced damping at the macroscale. Indentations may

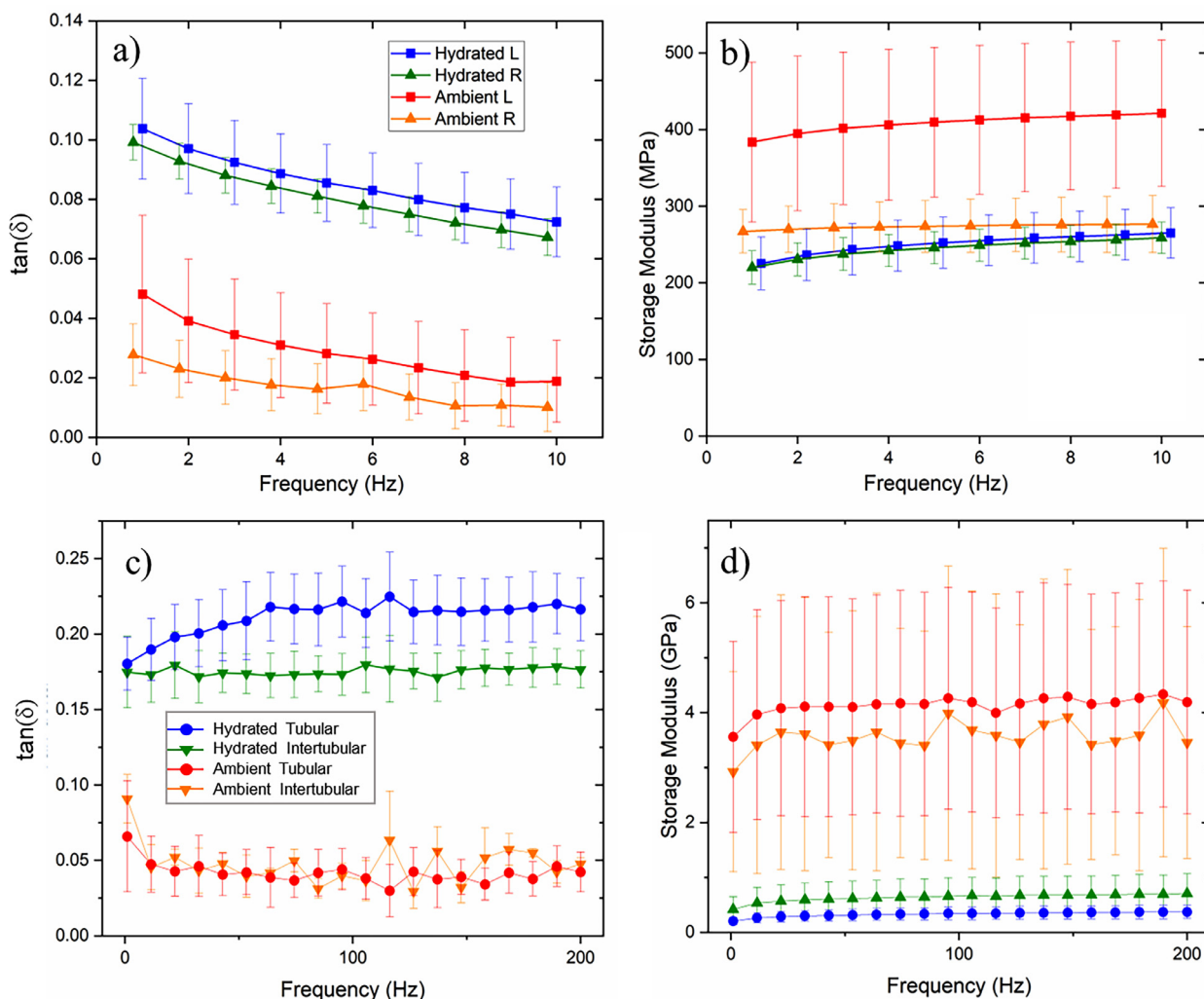


**Fig. 3.** Frequency sweep results for macroscale (a and b) and indentation (c and d) dynamic mechanical analysis of hoof wall material. Error bars refer to standard deviation. Data is aliased on the x-axis to avoid overlapping markers. L and R refer to longitudinal and radial directions, respectively.

also test an area that has a higher fraction of matrix compared to macroscale experiments that causes more sensitivity to hydration.

Hydrated hoof wall samples had lower storage and loss moduli with loss tangents 2–4 times higher than those tested in ambient air. The compliance of hydrated samples matches the trends observed in quasistatic tests [4,5,27]. The primary mechanism for the reduction in stiffness in hydrated  $\alpha$ -keratins is believed to be the breaking of hydrogen bonds in the keratin matrix by water molecules [32]. The matrix has a similar composition to IFs but is more sulfur-rich with higher cysteine content [33]. Rather than forming a highly crosslinked and crystalline structure like the IFs, the matrix is amorphous and held together by hydrogen bonds that break when surrounded by the highly polar water molecules [32,34]. This theory also explains the increased ductility and shape memory properties of hydrated keratins since the molecules of the matrix are free to break and switch hydrogen bonds [35]. The significantly higher loss modulus observed in hydrated samples is likely the result of non-conservative forces between molecules as they move past one another. The viscoelastic properties of IFs are unknown, but most evidence suggests that the pressure from the surrounding matrix constrains them from swelling and absorbing water [36,37]. Therefore, the increase in the hoof wall's viscous behavior in the fully hydrated condition is attributed to molecular changes in the matrix alone.

The insensitivity of IFs to hydration can explain the observed differences between the loss tangents of tubular and intertubular regions in nano-DMA experiments shown in Fig. 3c. According to birefringence measurements on the inner hoof wall, the IF content of both regions are close [38], but subsequent TEM measurements have indicated the IF volume fraction in the intertubular area (32 %) is larger than that of the tubular area (21 %) [5]. The properties of the tubule wall should be more sensitive to hydration if it has a lower fraction of IFs which matches our observations for loss tangent seen in Fig. 3c. The tubular region had a higher loss tangent than the intertubular material only when fully hydrated. Huang et al. observed a similar effect in the reduced moduli of the two regions measured with nanoindentation. Specifically, the tubular region was stiffer than the intertubular material when dry but more compliant when hydrated [5]. No significant difference between the storage modulus of the two regions was detected in this study. The comparison between storage moduli measurements and reduced moduli from previous work is not straightforward but both yielded similar values. for the elastic stiffness.

The loss tangent was lower in the radial direction for all frequencies of macroscale experiments. One might assume this is due to fiber orientation since IFs are expected to behave more elastically than the matrix [30]. If there was a preferred orientation of IFs in the hoof wall, any difference between the damping prop-

erties of IFs and the matrix would create anisotropy; however, the alignment of fibers is complicated and varies with location. Tubules are surrounded by concentric lamellae with alternating helically wound fibers at angles ranging from  $9^\circ$  to  $68^\circ$  from the tubule axes. For the intertubular material, fiber orientation changes along the radial direction. Near the stratum internum, intertubular fibers are perpendicular to the tubules but transition to be almost parallel to the tubules near the outer surface of the hoof wall [24]. Therefore, in the macroscopic samples tested in these experiments, which spanned almost the entire thickness, there is no obvious source of anisotropy due to fiber alignment.

The directional porosity of the tubules aligned in the longitudinal direction is also expected to have no effect on the loss tangent. Cellular solids can be modeled as a two-phase material with one phase consisting of empty space. The loss tangent of a cellular solid is the same as the solid material from which it is made [39,40]. This is true for both foams with random porosity and highly organized porosity such as honeycomb structures or the tubules in the hoof wall.

The difference in loss tangent cannot be explained by fluid flow within tubules either. If additional damping from fluid flow had a significant effect, the loss tangent of the radial direction would be higher since it is closer to the case of an open cell foam where energy can be dissipated by the movement of fluid through pores as opposed to longitudinal tests in which flow is restricted by the compression platens [41].

The tubules do, however, create anisotropy in stiffness leading to the lower storage moduli seen in the radial samples. In quasi-static tests, the hoof wall had the lowest stiffness in the radial direction at all hydration levels due to collapse of tubules along their minor axis [5,42]. Because of the tubule's orientation, the hoof wall behaves closer to a Voigt composite in the longitudinal direction and a Reuss composite in the radial direction. Similarly, the orientation of the tubules could create anisotropic damping, since the tubule wall and intertubular material exhibit different loss tangents. However, when the correspondence principle is applied to the Voigt and Reuss bounds, the hydrated material would have a higher loss tangent in the radial direction, which contrasts with observed results. Other features of the hoof wall may contribute to its anisotropy in damping such as the “waviness” of tubules. When they are compressed longitudinally, the wavy structure forces the tubules into bending or buckling deformation modes that could result in additional friction and damping that is not present during radial compression [42].

Previous research has demonstrated the effectiveness of the Generalized Maxwell model or Prony series in modeling the relaxation behavior of the hoof wall [4] and hair [30]. The parallel Maxwell elements in the model exhibit distinct time constants that are thought to represent the timescales of relaxation for different structural features within the hoof wall. Prony series models fitted to the dynamic frequency data presented in this work are unable to reproduce the relaxation curves from previous studies because of the large difference in strains between the two methods. Compression DMA was performed at  $< 1\%$  strain while relaxation experiments were done at strains of  $10\%$  or larger. Linear models such as Prony series are generally applicable over a small range of strains due to nonlinearity and plasticity that can occur in large deformations. *In vivo* measurements of hoof surface strains consistently report values well below  $1\%$  [21,43,44]. Therefore, a Prony series is adequate for most finite element studies of hoof wall deformation. However, it is important to note that for more specialized investigations involving anisotropy, localized deformation, fracture, and cumulative damage, advanced nonlinear models may be required. A more detailed discussion on fitting viscoelastic models to the experimental data presented here can be found in the Appendix.

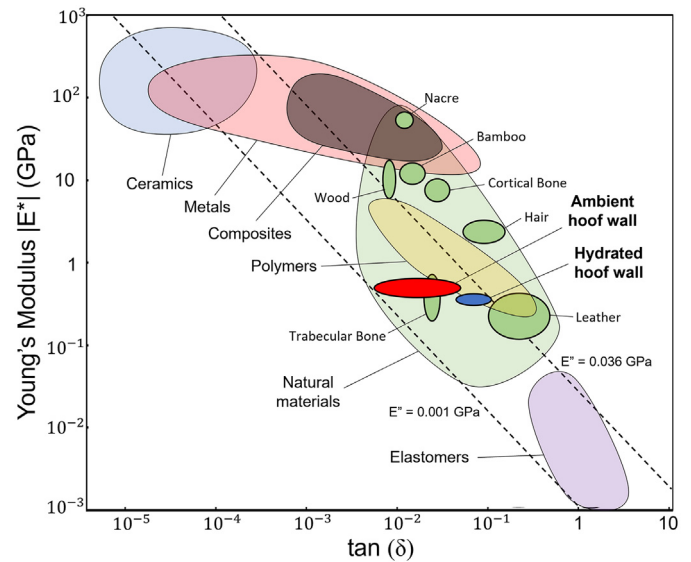


Fig. 4. Stiffness-loss map with results from macroscale DMA compression on hoof wall samples. Data taken from [30,48–52].

### 3.2. Statistical analysis

Results of the ANOVA are presented in Table 1. The P values represent the probability of making the given measurements if the factor has no effect on the property. If the P value is below the significance level of 0.05, then that factor has a statistically significant effect on the measured property.  $\eta_p^2$  is the proportion of the observed variation that can be explained by a given factor when accounting for all other variables in the model. Values above 0.14 are typically considered a large effect [45].

In addition to the factors previously discussed (hydration, loading direction, indentation location, and frequency), the ANOVA allows us to study the effect of variation between individual horses. Interestingly, the effect is low to medium in macroscale samples but undetectable in nano-DMA. This could be due to large variation in the results that reduce the power of the test.

### 3.3. Implications for impact resistance

The hoof wall, like all biological materials, is multifunctional, and evolved under many constraints that may not be present in engineering applications including thermal management, weight, limited constituent materials, and self-assembly. Its evolution has involved navigating various tradeoffs in mechanical performance that are manifested in substructures like layers, cells, and tubules, which enhance toughness at the expense of stiffness and strength [31].

The viscoelastic nature of the hoof wall introduces further trade-offs, especially in the context of impact resistance. This can be visualized by the stiffness-loss map depicted in Fig. 4, where a constant loss modulus is represented by a diagonal line. Materials with a high loss modulus (top right of Fig. 4) are desirable for attenuating vibrations because they can dissipate the most energy [40]. Meanwhile, materials with high loss tangents and low stiffness such as elastomers, generally reduce impact force [46]. However, under a mass or volume constraint, they are not necessarily best for protection from impact since a thin, compliant buffer would densify, offering no further benefit. Analytical studies have also highlighted the advantage of viscoelastic damping in reducing the maximum force experienced during impact. In a 1-dimensional buffer, a  $\tan(\delta)$  of 1 provides optimal force reduction [47].

**Table 1**  
ANOVA results.

Macroscale DMA		tan( $\delta$ )		Storage Modulus	
Factor	P	$\eta_p^2$	P	$\eta_p^2$	
Hydration	< 0.001*	0.855	< 0.001*	0.433	
Orientation (L or R)	< 0.001*	0.140	< 0.001*	0.170	
Frequency	< 0.001*	0.333	0.010*	0.025	
Animal	< 0.001*	0.082	0.023*	0.020	
Nano-DMA		tan( $\delta$ )		Storage Modulus	
Factor	P	$\eta_p^2$	P	$\eta_p^2$	
Hydration	< 0.001*	0.914	< 0.001*	0.557	
Location (Tubular or Intertubular)	< 0.001*	0.106	0.131	0.002	
Frequency	0.024*	0.004	0.010*	0.005	
Animal	0.823	< 0.001	0.150	0.003	

\* Signifies a statistically significant result ( $P < 0.05$ ).

From Fig. 4, it is clear the properties of the hoof wall do not maximize vibration attenuation or force reduction compared to other biological materials. Interestingly, the complex moduli of the ambient hoof wall are very close to measurements on trabecular bone [51], a material with a comparable mechanical function. Tension DMA on hair, which has a similar composition but very different microstructure, yielded larger storage modulus and loss tangent than ambient hoof wall material. Alignment of all fibers in the direction of loading accounts for the superior stiffness, but the exact values of complex moduli also seem to differ based on the specific structure and composition of the material. The loss tangent of human hair was greater than that of horsehair by more than a factor of 2 at the same frequency and hydration [30].

Ultimately, the hoof wall should not be considered an optimal material for protection from impact loading. Instead, it demonstrates a balance of stiffness and damping that is suitable for the survival of the organism. In addition to vibration attenuation and force reduction, a hoof wall must be durable, resistant to fracture, and have sufficient stiffness and compressive strength to support the weight of the animal. This unique combination of mechanical properties is achieved through its hierarchical organization, which modulates the effective properties at the macroscale with respect to those of the constituent materials. Some structures even exhibit multiple mechanical functions. Tubules, for example, reinforce the longitudinal direction [5], deflect incoming cracks [4], and absorb energy through reversible buckling and collapse of the medullary cavity [42]. Because of this multifunctionality and complexity, researchers must isolate and abstract individual structural mechanisms when developing bioinspired materials.

One such abstraction that should be considered for bioinspiration is functional gradation. The hoof wall has several features that vary along the radial direction such as IF volume fraction, tubule size, tubule density, stiffness, damping, and hydration. The convergence of these features on the same design motif indicates that there was evolutionary pressure to create a functionally graded structure. Spatially varying mechanical properties and morphology are not only prominent in the hoof wall, but also occur in other natural structures like bamboo [53] and horns [54]. Researchers have improved the performance of energy absorbing materials with gradients of stiffness [55,56] and porosity [57]. Functional gradients can be achieved by varying several factors including material composition, density, and architecture. The mechanisms of functionally graded structures differ by material and design but in the case of the hoof wall, the gradient in properties likely improves its resistance to localized impacts. The stiff exterior can resist local deformation, effectively spreading the contact area with the compliant hydrated material and reducing the reac-

tion stress transmitted to the soft tissue of the lamina. This work demonstrates there is also a significant gradient in damping that may contribute to dissipating energy and attenuating vibrations during impact to protect internal structures.

### 3.4. Limitations

Our study has several limitations that should be noted. First, the number of samples was limited due to the difficulty of obtaining equine hoof wall samples for mechanical testing. All samples used in this study were extracted from the hooves of a few individual horses. Significant variation is present between individuals, so more experiments are needed to determine the typical material behavior of the equine hoof wall. Meanwhile, the effects of age, weight, sex, and other factors on mechanical properties remain unknown. Moreover, the complex moduli presented in this work only apply to the linear viscoelastic region. Further characterization requires experiments at large deformations.

## 4. Conclusions

The equine hoof wall exhibits impressive mechanical performance and durability under impact loading. Previous research has examined the hoof wall's mechanical properties and hierarchical structure but lacks information on dynamic properties relevant to the loading rates experienced *in vivo*. This work characterized the linear viscoelastic behavior of the hoof wall with DMA and nano-DMA, resulting in the following conclusions:

1. Hydration, loading orientation, frequency, and animal all had a detectable effect on complex moduli. Hydration had the strongest effect in both macroscale and nano-DMA experiments.
2. The loss tangent of tubular regions was more sensitive to hydration than that of intertubular regions indicating a higher IF volume fraction in the intertubular material.
3. Nano-DMA resulted in higher effective stiffness and damping than macroscale experiments. The disparity is attributed to interfaces and pores not captured by nano-DMA and a difference in the IF volume fraction.
4. Radial compression resulted in lower storage moduli and loss tangents compared to the longitudinal direction. The oriented porosity of tubules is expected to create anisotropy in stiffness, but the source of anisotropic damping remains unclear.

### Declaration of AI and AI-assisted technologies in the writing process

During the preparation of this work the authors used GPT-4 to improve readability and clarity. After using this tool, the authors

reviewed and edited the content as needed and take full responsibility for the content of the publication.

### Declaration of competing interest

The authors declare that they have no known competing financial interests or personal relationships that could have appeared to influence the work reported in this paper.

### CRediT authorship contribution statement

**Christian Bonney:** Writing – original draft, Visualization, Validation, Methodology, Investigation, Formal analysis, Data curation, Conceptualization. **Siyuan Pang:** Writing – review & editing, Visualization, Investigation, Formal analysis, Data curation, Conceptualization. **Marc A. Meyers:** Writing – review & editing, Supervision, Investigation. **Iwona Jasiuk:** Writing – review & editing, Supervision, Resources, Project administration, Methodology, Investigation, Funding acquisition, Conceptualization.

### Acknowledgments

This research has been supported by the [National Science Foundation](#) Mechanics of Materials and Structures program (Grant numbers 1926353 and 1926361). We dedicate this paper to Prof. Joanna McKittrick's memory.

### Appendix

Linear viscoelastic models calibrated with low-strain data should be sufficient for most applications to equine biomechanics. The following appendix discusses fitting a Generalized Maxwell

model to the experimental data presented in this work. The Generalized Maxwell model, or Prony series, is a simple linear viscoelastic model available in most FEA software that can be represented by a spring in parallel with  $N$  Maxwell elements where  $N$  is the number of terms in the Prony series. For these models, the relaxation modulus can be written as:

$$E(t) = E_{\infty} + \sum_{i=1}^N E_i e^{-t/\tau_i} \quad (1-A)$$

A Prony series with two Maxwell elements fits the macroscale DMA data well; however, if we wish to model behavior for a larger range of timescales and loading rates, other experiments should be considered. Relaxation tests in the longitudinal direction were performed on ambient hoof samples with identical geometry to those used in DMA compression experiments. The samples were compressed in the longitudinal direction at a strain rate of  $10^{-2} \text{ s}^{-1}$  to a strain of 2.5 % and 5 % and held for 120 s. At these small strains the relaxation behavior is linear, i.e., the relaxation modulus does not depend on strain level as shown in Fig. A-1(a).

Prony series were fit to experimental stress relaxation and DMA compression data in the longitudinal direction using MCalibration software [58]. Relaxation, storage modulus, and loss modulus had equal weight in the Normalized Mean Absolute Difference (NMAD), which was minimized during fitting. Fig. A-1 (b-c) shows the Prony series predictions after fitting along with the experimental data. With 5 or more terms, the full behavior is captured with low error (NMAD < 5). The models tend to underpredict storage modulus and overpredict loss modulus but well within the variation seen from experiments. The fit is improved by additional elements with diminishing returns after about 5 terms.

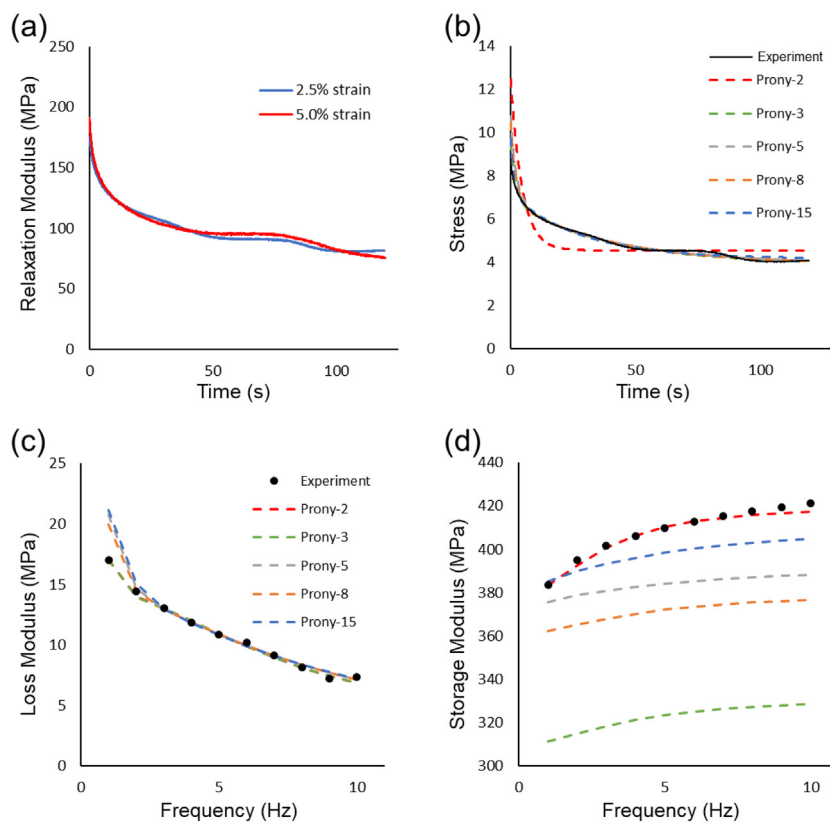


**Fig. A-1.** (a) Relaxation modulus of ambient samples compressed to 2.5 % and 5 % strain. (b-d) Experimental data for the ambient condition fitted to Prony series models. Prony- $N$  refers to a Prony series with  $N$  terms.

More advanced models can be applied to the data presented here. Specifically, models accounting for nonlinearity at large deformations, anisotropy, and damage would provide the most accurate representation of hoof wall material behavior.

## References

- [1] B. Wang, B. Zhou, X. Zhang, A high toughness and light weight armor structure bioinspired design based on a bovine hoof wall, *Mater. Lett.* 264 (2020) 127296, doi:10.1016/j.matlet.2020.127296.
- [2] C. Rice, K. Tan, Horse hoof inspired biomimetic structure for improved damage tolerance and crack diversion, *Comp. Struct.* 220 (2019) 362–370, doi:10.1016/j.compstruct.2019.04.009.
- [3] W. Ma, S. Xie, Z. Li, Mechanical performance of bio-inspired corrugated tubes with varying vertex configurations, *Int. J. Mech. Sci.* 172 (2020) 105399, doi:10.1016/j.ijmecsci.2019.105399.
- [4] B.S. Lazarus, R.K. Luu, S. Ruiz-Pérez, W.B.A. Bezerra, K. Becerra-Santamaria, V. Leung, V.H.L. Durazo, I. Jasiuk, J.D. Barbosa, M.A. Meyers, Equine hoof wall structure, properties, and bioinspired designs, *Acta Biomater.* 151 (2022) 426–445, doi:10.1016/j.actbio.2022.08.028.
- [5] W. Huang, N.A. Yaraghi, W. Yang, A. Velazquez-Olivera, Z. Li, R.O. Ritchie, D. Kisailus, S.M. Stover, J. McKittrick, A natural energy absorbent polymer composite: the equine hoof wall, *Acta Biomater.* 90 (2019) 267–277, doi:10.1016/j.actbio.2019.04.003.
- [6] M.A. Kasapi, J.M. Gosline, Strain-rate-dependent mechanical properties of the equine hoof wall, *J. Exp. Biol.* 199 (5) (1996) 1133–1146, doi:10.1242/jeb.199.5.1133.
- [7] S. Barnes, D. Shepherd, D. Espino, R. Bryan, Frequency dependent viscoelastic properties of porcine bladder, *J. Mech. Behav. Biomed. Mater.* 42 (2015) 168–176, doi:10.1016/j.jmbm.2014.11.017.
- [8] F.S. Julie, H.T. Strøm, P. Mette, G. Hans, N.J. Vinge, Dynamic viscoelastic properties of porcine gastric tissue: effects of loading frequency, region and direction, *J. Biomech.* 143 (2022) 111302, doi:10.1016/j.jbiomech.2022.111302.
- [9] A. Kumar, I.A.I. Matari, S.S. Han, 3d printable carboxylated cellulose nanocrystal-reinforced hydrogel inks for tissue engineering, *Biofabrication* 12 (2) (2020) 025029, doi:10.1088/1758-5090/ab736e.
- [10] A.-M.M. Persson, E.L. Hinrichsen, E. Andreassen, On the temperature dependence of the cyclic compression behaviour of a thermoplastic vulcanizate elastomer, *Polym. Test.* 112 (2022) 107650, doi:10.1016/j.polymertesting.2022.107650.
- [11] S. Wang, Y. Ma, Z. Deng, S. Zhang, J. Cai, Effects of fused deposition modeling process parameters on tensile, dynamic mechanical properties of 3d printed polylactic acid materials, *Polym. Test.* 86 (2020) 106483, doi:10.1109/Diagnostika49114.2020.9214627.
- [12] K.P. Menard, N. Menard, *Dynamic Mechanical Analysis*, CRC Press, 2020.
- [13] C. Anthony, *Nanoindentation*, Springer, New York, 2011.
- [14] H. Chateau, L. Holden, D. Robin, S. Falala, P. Pourcelot, P. Estoup, J.M. Denoix, N. CREVIER-DENOIX, Biomechanical analysis of hoof landing and stride parameters in harness trotter horses running on different tracks of a sand beach (from wet to dry) and on an asphalt road, *Equine Vet. J.* 42 (2010) 488–495, doi:10.1111/j.2042-3306.2010.00277.x.
- [15] J.J. Setterbo, T.C. Garcia, I.P. Campbell, J.L. Reese, J.M. Morgan, S.Y. Kim, M. Hubbard, S.M. Stover, Hoof accelerations and ground reaction forces of thoroughbred racehorses measured on dirt, synthetic, and turf track surfaces, *Am. J. Vet. Res.* 70 (10) (2009) 1220–1229, doi:10.2460/ajvr.70.10.1220.
- [16] T. Witte, C. Hirst, A. Wilson, Effect of speed on stride parameters in racehorses at gallop in field conditions, *J. Exp. Biol.* 209 (21) (2006) 4389–4397, doi:10.1242/jeb.02518.
- [17] P. Benoit, E. Barrey, J. Regnault, J. Brochet, Comparison of the damping effect of different shoeing by the measurement of hoof acceleration, *Cells Tissues Org.* 146 (2–3) (1993) 109–113, doi:10.1159/000147430.
- [18] C. Hinterhofer, C. Stanek, H. Haider, The effect of flat horseshoes, raised heels and lowered heels on the biomechanics of the equine hoof assessed by finite element analysis (fea), *J. Vet. Med. Ser. A* 47 (2) (2000) 73–82, doi:10.1046/j.1439-0442.2000.00263.x.
- [19] C. Hinterhofer, C. Stanek, H. Haider, Finite element analysis (fea) as a model to predict effects of farriery on the equine hoof, *Equine Vet. J.* 33 (S33) (2001) 58–62, doi:10.1111/j.2042-3306.2001.tb05360.x.
- [20] M. Jansová, L. Ondoková, J. Vychytil, P. Kochová, K. Witter, Z. Tonar, A finite element model of an equine hoof, *J. Equine Vet. Sci.* 35 (1) (2015) 60–69, doi:10.1016/j.jevs.2014.11.008.
- [21] N.A. Shahkhosravi, M.C. Bellenzani, H.M. Davies, A. Komeili, The influence of equine limb conformation on the biomechanical responses of the hoof: an *in vivo* and finite element study, *J. Biomech.* 128 (2021) 110715, doi:10.1016/j.jbiomech.2021.110715.
- [22] M.A. Kasapi, *Design for Fracture Control and the Mechanical Properties of the Equine Hoof Wall*, University of British Columbia, 1997.
- [23] J. McKittrick, P.-Y. Chen, S. Bodde, W. Yang, E. Novitskaya, M. Meyers, The structure, functions, and mechanical properties of keratin, *JOM* 64 (4) (2012) 449–468, doi:10.1007/s11837-012-0302-8.
- [24] M.A. Kasapi, J.M. Gosline, Design complexity and fracture control in the equine hoof wall, *J. Exp. Biol.* 200 (11) (1997) 1639–1659, doi:10.1242/jeb.200.11.1639.
- [25] M.A. Mahrous, C. Chadha, P.L. Robins, C. Bonney, K.A. Boateng, M. Meyers, I. Jasiuk, Multimodule imaging of the hierarchical equine hoof wall porosity and structure, *J. Mater. Res. Tech.* 26 (2023) 5535–5548, doi:10.1016/j.jmrt.2023.08.246.
- [26] J. Bertram, J. Gosline, Functional design of horse hoof keratin: the modulation of mechanical properties through hydration effects, *J. Exp. Biol.* 130 (1) (1987) 121–136, doi:10.1242/jeb.130.1.121.
- [27] D.H. Leach, *The Structure and Function of the Equine Hoof Wall*, University of Saskatchewan, 1980.
- [28] J. Reilly, D. Cottrell, R. Martin, D. Cuddeford, Tubule density in equine hoof horn, *Biomimetics* 4 (1996) 23–36.
- [29] V. Placet, E. Foltete, Is dynamic mechanical analysis (dma) a non-resonance technique? in: EPJ Web Conferences, 2010, p. 41004. EDP Sciences.
- [30] Y. Yu, W. Yang, M.A. Meyers, Viscoelastic properties of  $\alpha$ -keratin fibers in hair, *Acta Biomater.* 64 (2017) 15–28, doi:10.1016/j.actbio.2017.09.012.
- [31] C.-S.A. Shiang, C. Bonney, B. Lazarus, M. Meyers, I. Jasiuk, Hierarchical modeling of elastic moduli of equine hoof wall, *J. Mech. Behav. Biomed. Mater.* 136 (2022) 105529, doi:10.1016/j.jmbm.2022.105529.
- [32] W. Huang, A. Zaheri, W. Yang, D. Kisailus, R.O. Ritchie, H. Espinosa, J. McKittrick, How water can affect keratin: hydration-driven recovery of bighorn sheep (*ovis canadensis*) horns, *Adv. Funct. Mater.* 29 (27) (2019) 1901077, doi:10.1002/adfm.201901077.
- [33] J. Gillespie, M. Frenkel, The diversity of keratins, *Compar. Biochem. Physiol. Part B: Compar. Biochem.* 47 (2) (1974) 339–346, doi:10.1016/0305-0491(74)90063-7.
- [34] B.C. Powell, G.E. Rogers, *Hair keratin: composition, structure and biogenesis*, in: *Biology of the Integument: 2 Vertebrates*, Springer, 1986, pp. 695–721.
- [35] T.N. Sullivan, Y. Zhang, P.D. Zavattieri, M.A. Meyers, Hydration-induced shape and strength recovery of the feather, *Adv. Funct. Mater.* 28 (30) (2018) 1801250, doi:10.1002/adfm.201801250.
- [36] D.S. Fudge, J.M. Gosline, Molecular design of the  $\alpha$ -keratin composite: insights from a matrix-free model, hagfish slime threads, *Proc. R. Soc. Lond. Ser. B: Biol. Sci.* 271 (1536) (2004) 291–299, doi:10.1098/rspb.2003.2591.
- [37] D.A. Greenberg, D.S. Fudge, Regulation of hard  $\alpha$ -keratin mechanics via control of intermediate filament hydration: matrix squeeze revisited, *Proc. R. Soc. B: Biol. Sci.* 280 (1750) (2013) 20122158, doi:10.1002/advs.202400255.
- [38] M.A. Kasapi, J.M. Gosline, Micromechanics of the equine hoof wall: optimizing crack control and material stiffness through modulation of the properties of keratin, *J. Exp. Biol.* 202 (4) (1999) 377–391, doi:10.1242/jeb.202.4.377.
- [39] S. Amada, R. Lakes, Viscoelastic properties of bamboo, *J. Mater. Sci.* 32 (1997) 2693–2697, doi:10.1186/s10086-020-01914-y.
- [40] R.S. Lakes, *Viscoelastic Materials*, Cambridge University Press, 2009.
- [41] M. Rodriguez-Perez, M. Álvarez-Láinez, J. De Saja, Microstructure and physical properties of open-cell polyolefin foams, *J. Appl. Polym. Sci.* 114 (2) (2009) 1176–1186, doi:10.1002/app.30283.
- [42] B.S. Lazarus, R.K. Luu, S. Ruiz-Pérez, J.D. Barbosa, I. Jasiuk, M.A. Meyers, Equine hoof wall deformation: novel aspects revealed, *Small Struct* 4 (10) (2023) 2200402, doi:10.1002/sstr.202200402.
- [43] J. Thomason, W. Bignell, W. Sears, Components of variation of surface hoof strain with time, *Equine Vet. J.* 33 (S33) (2001) 63–66, doi:10.1111/j.2042-3306.2001.tb05361.x.
- [44] J. Thomason, A. Cruz, W. Bignell, D. Redman, S. Jackson, *In situ strain measurement on the equine hoof*, in: *Proceedings of the 2007 SEM Annual Conference and Exposition, Society for Experimental Mechanics, Springfield (MA)*, 2007.
- [45] H.-Y. Kim, Statistical notes for clinical researchers: sample size calculation 3. Comparison of several means using one-way anova, *Restor. Dent. Endod.* 41 (3) (2016) 231–234, doi:10.5395/rde.2016.41.3.231.
- [46] M. Benanti, L. Andena, F. Briatico-Vangosa, A. Pavan, Viscoelastic behavior of athletics track surfaces in relation to their force reduction, *Polym. Test.* 32 (1) (2013) 52–59, doi:10.1016/j.polymertesting.2012.09.008.
- [47] C. Chen, R. Lakes, Design of viscoelastic impact absorbers: optimal material properties, *Int. J. Solid. Struct.* 26 (12) (1990) 1313–1328, doi:10.1016/0020-7683(90)90081-6.
- [48] R. Lakes, High damping composite materials: effect of structural hierarchy, *J. Comp. Mater.* 36 (3) (2002) 287–297, doi:10.1177/0021998302036003538.
- [49] W. Woigk, K. Masania, F. Stork, A. Heusi, E. Poloni, A.R. Studart, Bio-inspired platelet-reinforced polymers with enhanced stiffness and damping behavior, *ACS Appl. Polym. Mater.* 2 (8) (2020) 3557–3565, doi:10.1021/acsapm.0c00568.
- [50] W. Woigk, E. Poloni, M. Grossman, F. Bouville, K. Masania, A.R. Studart, Nacre-like composites with superior specific damping performance, *Proc. Nat. Acad. Sci.* 119 (31) (2022) e2118868119, doi:10.1073/pnas.2118868119.
- [51] J. Yamashita, B.R. Furman, H.R. Rawls, X. Wang, C.M. Agrawal, The use of dynamic mechanical analysis to assess the viscoelastic properties of human cortical bone, *J. Biomed. Mater. Res.: Off. J. Soc. Biomater. Jpn. Soc. Biomater. Aust. Soc. Biomater.* 58 (1) (2001) 47–53, doi:10.1002/1097-4636(2001)58:1(47::AID-JBM70)3.0.CO;2-U.
- [52] D. Ronca, A. Gloria, R. De Santis, T. Russo, U. D'Amora, M. Chierchia, L. Nicolais, L. Ambrosio, Critical analysis on dynamic-mechanical performance of spongy bone: the effect of an acrylic cement, *Hard Tissue* 3 (1) (2014) 9–16.
- [53] M.K. Habibi, L.-h. Tam, D. Lau, Y. Lu, Viscoelastic damping behavior of structural bamboo material and its microstructural origins, *Mech. Mater.* 97 (2016) 184–198, doi:10.1016/j.mechmat.2016.03.002.
- [54] M.W. Trim, M. Horstemeyer, H. Rhee, H. El Kadiri, L.N. Williams, J. Liao, K.B. Walters, J. McKittrick, S.-J. Park, The effects of water and microstructure on the mechanical properties of bighorn sheep (*ovis canadensis*) horn keratin, *Acta Biomater.* 7 (3) (2011) 1228–1240, doi:10.1016/j.actbio.2010.11.024.
- [55] J. Ma, J. Song, Y. Chen, An origami-inspired structure with graded stiffness, *Int. J. Mech. Sci.* 136 (2018) 134–142, doi:10.1016/j.ijmecsci.2017.12.026.

- [56] H. Niknam, A. Akbarzadeh, Graded lattice structures: simultaneous enhancement in stiffness and energy absorption, *Mater. Design* 196 (2020) 109129, doi:[10.1016/j.matdes.2020.109129](https://doi.org/10.1016/j.matdes.2020.109129).
- [57] K.Z. Uddin, G. Youssef, M. Trkov, H. Seyyedhosseinzadeh, B. Koohbor, Gradient optimization of multi-layered density-graded foam laminates for footwear material design, *J. Biomech.* 109 (2020) 109950, doi:[10.1016/j.jbiomech.2020.109950](https://doi.org/10.1016/j.jbiomech.2020.109950).
- [58] J. Bergstrom, *Polyumod—a Library of Advanced User Materials*, Veryst Engineering, LLC, Needham, Mass, USA, 2012.